Wind Energ. Sci., 1, 41–53, 2016
www.wind-energ-sci.net/1/41/2016/
doi:10.5194/wes-1-41-2016

eawe european academy of wind energy
Open Access
WIND ENERGY SCIENCE

Full-field assessment of wind turbine near-wake deviation in relation to yaw misalignment

Juan José Trujillo[1], Janna Kristina Seifert[1], Ines Würth[2], David Schlipf[2], and Martin Kühn[1]

[1]ForWind – University of Oldenburg, Institute of Physics, Ammerländer-Heerstr. 136, 26129 Oldenburg, Germany
[2]Stuttgart Wind Energy at University of Stuttgart, Institute of Aircraft Design, Allmandring 5B, 70569 Stuttgart, Germany

Correspondence to: Juan José Trujillo (juan.jose.trujillo@uni-oldenburg.de)

Received: 30 December 2015 – Published in Wind Energ. Sci. Discuss.: 19 January 2016
Revised: 26 March 2016 – Accepted: 1 April 2016 – Published: 11 April 2016

Abstract. Presently there is a lack of data revealing the behaviour of the path followed by the near wake of full scale wind turbines and its dependence on yaw misalignment. Here we present an experimental analysis of the horizontal wake deviation of a 5 MW offshore wind turbine between 0.6 and 1.4 diameters downstream. The wake field has been scanned with a short-range lidar and the wake path has been reconstructed by means of two-dimensional Gaussian tracking. We analysed the measurements for rotor yaw misalignments arising in normal operation and during partial load, representing high thrust coefficient conditions. We classified distinctive wake paths with reference to yaw misalignment, based on the nacelle wind vane, in steps of 3° in a range of ±10.5°. All paths observed in the nacelle frame of reference showed a consistent convergence towards 0.9 rotor diameters downstream, suggesting a kind of wake deviation shift. This contrasts with published results from wind tunnels which in general report a convergence towards the rotor. The discrepancy is evidenced in particular in a comparison which we performed against published paths obtained by means of tip vortex tracking.

1 Introduction

Lately, attention has been directed towards the effects of wind turbine misalignment on wake aerodynamics. Wind tunnel experiments (e.g. Medici and Dahlberg, 2003) and numerical simulations (e.g. Jiménez et al., 2010; Fleming et al., 2014) suggest that the steady path followed by a wind turbine wake can be regulated actively. Consequently, it is envisioned to optimise the wake path of individual wind turbines to increase the overall efficiency of a wind farm. One of the techniques proposed to achieve this relies on the active control of the wake lateral position by means of active inducement of rotor yaw misalignment. The aim is to avoid full wake effects for wind directions of perfect turbine alignment by means of control strategies taking into account the global wind farm performance; see, for instance, the work of Gebraad et al. (2016) and Fleming et al. (2016). At present, questions have arisen regarding the transferability of the findings of the controlled lab and numerical experiments to the full field. The experimental study of the deviation effect is not simple since the wake flow has to be measured comprehensively in time and space. Therefore, special measuring techniques have to be applied in order to resolve the flow field in a spatial domain covering a substantial part of the wake to finally estimate the wake position along its downstream path.

In wind tunnel experiments the quantification of the wake path is performed by means of tip vortex tracking (e.g. Grant et al., 1997; Medici and Dahlberg, 2003; Haans et al., 2005). The technique is based on visualisation of passive tracers revealing the deviation of vortex generated at the blade tips. Additionally, techniques which reveal the full wake flow using particle image velocimetry (PIV) are also applied (e.g. Krogstad and Adaramola, 2012; Rockel et al., 2014). In spite of their suitability in the lab, these visualisation techniques are, to our knowledge, not applicable at the scales of modern commercial wind turbines. A full-field alternative tech-

nique is the application of remote sensing techniques. Together with other researchers the first author of this paper proposed a wake-tracking technique in Trujillo et al. (2011) which is based on two-dimensional lidar measurements from the wind turbine nacelle. In that research the technique is applied in the far wake at four diameters ($4\,\mathcal{D}$) downstream of a medium-scale wind turbine. Others have applied a similar methodology, of fitting a predefined wake shape to lidar data, in order to capture the far-wake path of large-scale wind turbines (e.g. Aitken et al., 2014; Machefaux et al., 2015). However, we have not found literature about experimental studies in the near wake between the rotor and $2\,\mathcal{D}$ downstream relating to yaw misalignment effects. Such measurements are useful to understand the wake behaviour in its full extent and for validation of findings with physical and numerical models. Moreover, such measurements should give insight into the relation of measurements in the vicinity of the rotor, for instance the nacelle wind vane, and the wake deviation. This is helpful regarding the future needs in sensors for implementation of active wake control strategies.

In this research we aim to measure horizontal near-wake paths and observe the dependence of their trajectory on yaw misalignment by applying nacelle-based wake-tracking techniques. The investigation is based on data processed for a proof of concept presented orally at the conference of the European Wind Energy Association in March 2014 under the title "Measuring wind turbine yaw misalignment by wake tracking" and with the same authorship as this paper. Initially we revise a wake-tracking technique already used in far-wake studies. Then, we show statistics of wake position tracked between 0.6 and $1.4\,\mathcal{D}$ downstream of an offshore wind turbine. In a next step, we estimate wake paths and classify them with respect to yaw misalignment conditions arising in normal operation. Furthermore, we discuss the factors that may affect the measurement technique and the results. Finally, we compare the findings against results from a published wind tunnel experiment applying vortex tracking in a region from $0.2\,\mathcal{D}$ to $0.5\,\mathcal{D}$ downstream.

2 Methods

2.1 Near-wake path reconstruction from wake tracking

The path followed by the wake of a wind turbine can be reconstructed by estimating the transversal position of the wake deficit at a discrete number of downstream stations. At present, this can be performed in the full field by applying wake tracking on wind fields obtained with nacelle-based scanning lidars. In this method the bulk transversal location of the wind speed deficit is identified at each downstream station. For this, the wind velocity is measured on sections parallel to the turbine rotor at defined downstream stations. Figure 1 shows this with the convention for positive yaw misalignment. There, the subscript "l" stands for the lidar frame of reference, which is attached to the measurement system.

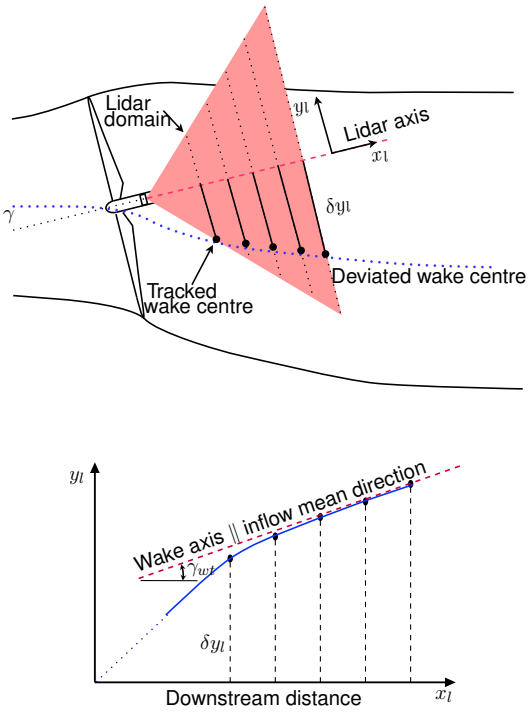

Figure 1. Sketch of near-wake path reconstruction. Top panel: top view of lidar wake tracking. Shadowed area shows the area which is covered by a lidar system aligned with the rotor axis. Perpendicular dotted lines represent one-dimensional or two-dimensional scans parallel to the rotor. Dots depict estimated wake centres. Bottom panel: reconstruction of near-wake path and estimation of yaw misalignment based on discrete measurements. Lidar frame of reference (subscript "l") assumed perfectly aligned with the nacelle axis.

This frame of reference can be assumed equal to a nacelle frame of reference if a perfect alignment between the lidar and the nacelle is assumed. Afterwards, the wake offset in lateral direction ($\delta\, y_l$) is estimated at each station. The average over a defined period of time of the wake offsets, at each downstream position, describes the near-wake path.

2.2 Lidar wake tracking with bivariate Gaussian templates

Several procedures can be applied to estimate a wake centre position based on lidar measurements. For instance, with image processing techniques the wake limits, and consequently a wake centre, can be identified by using a wind speed threshold defining the inner and outer part of the wake; such a technique has been applied by España et al. (2011) on PIV measurements in the wind tunnel. Another approach is to fit the measured wind field to an expected shape of the wind speed distribution across the wake. The selected shape includes a wake position marker among other parameters with or without physical meaning. We find two examples of this, namely the approach by Trujillo et al. (2011), whose objective is to

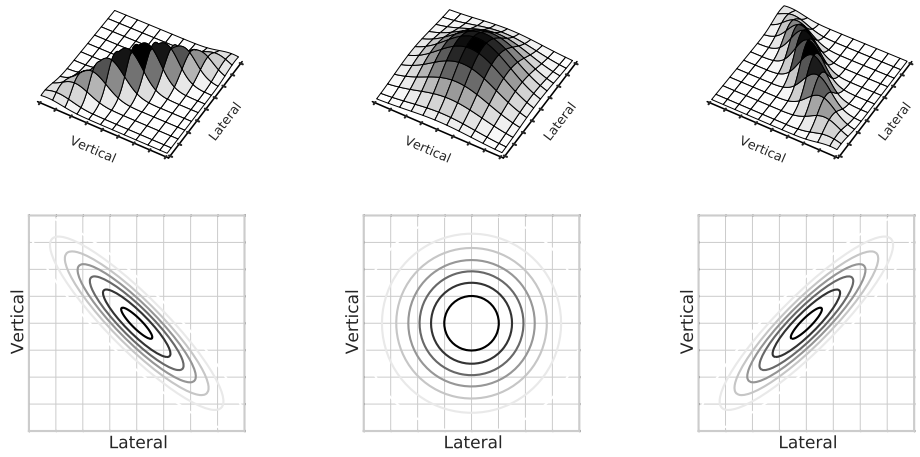

Figure 2. Example of bivariate function (Eq. 1) for equal parameters μ_y, μ_z, σ_y, σ_z, and A, but varying correlation values as $\rho = -0.9$, $\rho = 0$, and $\rho = 0.9$, respectively, from left to right. Top panels represent the wake speed deficit and bottom panels the contour lines.

find the best fit between a template function and the wind speed distribution, and the approach applied by Aitken et al. (2014), where the best fit of a flow model is searched.

In this research we employed a slightly modified version of the wake-tracking technique from Trujillo et al. (2011). That method has been developed for analysis of two-dimensional lidar measurements in the far wake. The main difference with the published research is that we used here the non-simplified fitting function and formulated an additional function for more complex flow. In the following we re-introduce the method and illustrate the additions we make. In the tracking procedure, wind field snapshots are taken across the wake on vertical planes parallel to the rotor. Next, wind speed deficits are calculated by subtracting the average inflow vertical profile measured at an additional system, such as a meteorological mast or forward-looking lidar. This procedure intends to isolate the deficit in order to reduce the asymmetry created by the vertical shear and make it more suitable for the final process, where a bivariate Gaussian function (Eq. 1) is fitted by means of least squares to each wind speed deficit.

$$f\left(y_i, z_i | \mu_y, \mu_z, \sigma_y, \sigma_z, A, \rho\right) = \frac{A}{2\pi\sigma_y\sigma_z\sqrt{1-\rho^2}} \cdot \exp\left[-\frac{1}{2\left(1-\rho^2\right)}\left(\frac{\left(y_i-\mu_y\right)^2}{\sigma_y^2} - \frac{2\rho\left(y_i-\mu_y\right)\left(z_i-\mu_z\right)}{\sigma_y\sigma_z} + \frac{\left(z_i-\mu_z\right)^2}{\sigma_z^2}\right)\right] \quad (1)$$

The Gaussian function is selected as a fitting template due to its flexibility to adapt to axial-symmetric or non-axial-symmetric shapes. This is convenient in the near wake since the quasi-instantaneous velocity across the rotor is characterised by a complex shape. Furthermore, in the case of analysis of steady wake profiles, this function should describe better the expected wake speed profile for different downstream distances; see, for instance, a review of the wake fields obtained by means of numerical and wind tunnel experiments documented by Vermeer et al. (2003). The target is to obtain the best estimate of μ_y and μ_z, which define the axis of the Gaussian function. This is assumed to be a marker of the wake centre location in horizontal (y) and vertical (z) direction. The parameters σ_y and σ_z characterise the shape lateral and vertical width, respectively. Moreover, ρ represents the correlation between both coordinates and its magnitude ($|\rho|$) is lesser than 1. In the case that the axes of elongation and compression of the shape are aligned with y and z, ρ is 0; otherwise this parameter generates a rotation of the axes (Fig. 2). We expect this parameter to be useful in capturing non axisymmetric wake shapes, for instance those attributed to wake rotational effects. Furthermore, it is expected that this shape fits in a robust manner with deficits with complex shapes due to uneven induction, rotational effects, and boundary layer interaction.

Additionally, the near-wake flow is characterised by the detailed rotor aerodynamics. In particular, the low induction at the blade root lets wind pass the rotor almost unaffected. This is expressed in a wind speed peak in the near-wake centre which we propose to capture by subtracting a concentric Gaussian function from Eq. (1). The resulting function can be seen in Eq. (2), where the second term on the right-hand side (subscript 2) is subtracted from Eq. (1) (subscript 1). This creates a depression at the highest values of the single Gaussian form describing the wake deficit (see Fig. 3).

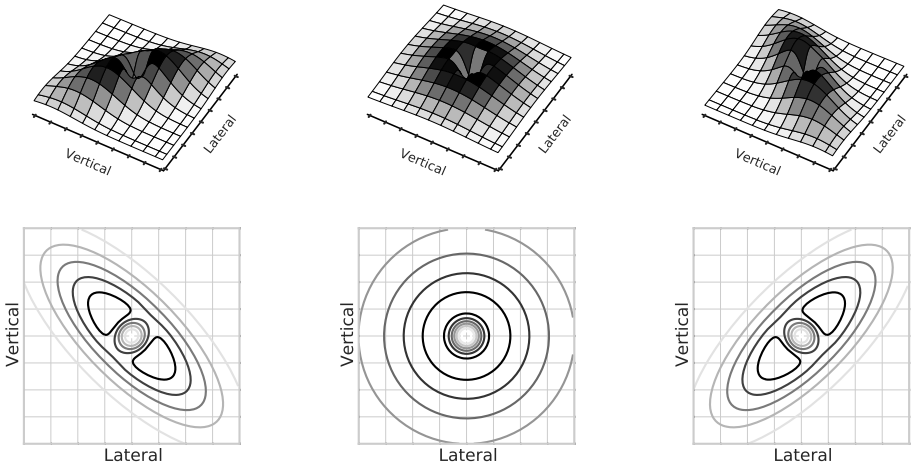

Figure 3. Example of extended bivariate function (Eq. 2) for equal parameters μ_y, μ_z, σ_{y_1}, σ_{y_2}, σ_{z_1}, σ_{z_2}, A_1, and A_2, but varying correlation values as $\rho = -0.9$, $\rho = 0$, and $\rho = 0.9$, respectively, from left to right. Top panels represent the wake speed deficit and bottom panels the contour lines.

$$
\begin{aligned}
&f\left(y_i, z_i | \mu_y, \mu_z, \sigma_{y_1}, \sigma_{y_2}, \sigma_{z_1}, \sigma_{z_2}, A_1, A_2, \rho_1\right) \\
&= \frac{A_1}{2\pi\sigma_{y_1}\sigma_{z_1}\sqrt{1-\rho_1^2}} \cdot \exp\left[-\frac{1}{2\left(1-\rho^2\right)}\right. \\
&\left.\left(\frac{\left(y_i-\mu_y\right)^2}{\sigma_{y_1}^2} - \frac{2\rho\left(y_i-\mu_y\right)\left(z_i-\mu_z\right)}{\sigma_{y_1}\sigma_{z_1}} + \frac{\left(z_i-\mu_z\right)^2}{\sigma_{z_1}^2}\right)\right] \\
&- \frac{A_2}{2\pi\sigma_{y_2}\sigma_{z_2}} \exp\left[-\frac{1}{2}\left(\frac{\left(y_i-\mu_y\right)^2}{\sigma_{y_2}^2} + \frac{\left(z_i-\mu_z\right)^2}{\sigma_{z_2}^2}\right)\right] \qquad (2)
\end{aligned}
$$

The two functions presented here show a formal similarity with the approach applied by Aitken et al. (2014), although extended to two-dimensional measurements. However, both procedures differ in principle since our method does not strive to reproduce the model behind the measurements but to identify the existence and location of a bell-like shape. This allows us to even perform tracking directly on line-of-sight measurements without the need of reconstructing the full wind field. This has been tested in a computational setup with large eddy simulation, actuator line for turbine simulation, and lidar simulator in Trabucchi et al. (2011). More specifically, the wake of a model of a 2 MW wind turbine has been scanned at $2.5\,\mathcal{D}$ downstream with nacelle-based and ground-based lidars. The results showed for the simulated test case that the wake tracking applied on line-of-sight wind speeds predicts similar wake position than the reference tracking based on the full wind field with average deviations below 1.5 %. Furthermore the study showed a robust behaviour for large misalignments between the mean line-of-sight and the mean wind direction ranging from 0 to 60°.

3 Full-field experiment at "alpha ventus" offshore wind farm

We applied the techniques for near-wake path reconstruction to measurements performed on a wind turbine at the offshore test wind farm "alpha ventus". The measurement campaign took place from 3 March 2011 until 25 July 2011. Measurement data have been selected and synchronised as 10 min averages from three different measurement systems. That is, the turbine data were obtained from the supervisory control and data acquisition (SCADA) system, the lidar scanner provided the wake wind field data; finally, the inflow data are recorded from a meteorological mast located at the offshore research platform FINO1.

3.1 Wind turbine and nacelle-based lidar system

The studied turbine is the AV07, which is located in the third row from top to bottom and on the westerly side (shown as a square in Fig. 4). This turbine is of type Adwen AD 5-116, formerly called M5000-116. It has a rotor diameter ($\mathcal{D}$) of 116 m and a hub height of 90 m. The cut-in wind speed is $3.5\,\mathrm{m\,s^{-1}}$, the nominal wind speed is $12.5\,\mathrm{m\,s^{-1}}$, and the cut-out wind speed $25.0\,\mathrm{m\,s^{-1}}$.

Wind turbine data were provided by the SCADA system with a 1 min sampling rate. Mainly, we recorded the nacelle wind vane as the yaw misalignment sensor and estimate a proxy status signal. We estimated this status as an on/off signal by evaluating 10 min averages of power production and generator rotational speed. Finally, we processed the data in blocks of 10 min without checking yaw manoeuvres of the turbine in each period of time. We took the decision to skip this check because of practical reasons; for instance, this would force us to work with data blocks shorter than 10 min

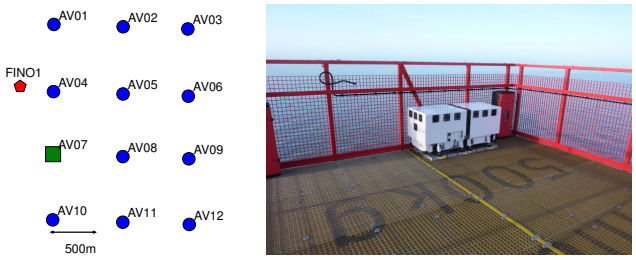

Figure 4. Measurement system installation at alpha ventus. Left panel: layout of alpha ventus wind farm and position of FINO1 meteorological mast. Right panel: photography of installation of Windcube plus scanner at helicopter deck of the Adwen's AD 5-116.

and variable in size, leading to issues of inflow steadiness with respect to the reference meteorological mast.

The wind turbine near wake has been measured with a research scanning lidar. The system is equipped with a commercial short-range pulsed lidar of type Windcube WLS-7 version 1.0 from the manufacturer Leosphere. This is coupled to a scanner with 2 degrees of freedom, which has been designed by the research group Stuttgart Wind Energy at the University of Stuttgart. The lidar was located on top of the nacelle on the rear part of the helicopter deck of the AV07, as can be observed in Fig. 4. The position of the source of the lidar, which is the pivot of the scanner mirror, has been estimated as $x = 4.3\,\mathrm{m}$, $y = -1.1\,\mathrm{m}$, and $z = 3.5$ m on the nacelle frame of reference. This is a right-hand frame which is centred at the intersection of the tower and the rotor axis and whose x axis points downstream. We estimated that an orientation error in the alignment of the lidar scanning axis with reference to the nacelle longitudinal axis is in the order of $\pm 1°$. More details of this system can be found in Peña et al. (2013, chap. 8).

The lidar system measures at five stations downstream, namely, 0.6, 0.8, 1.0, 1.2, and $1.4\,\mathcal{D}$, which here are numbered from 1 to 5, respectively. The scanning is performed in a quasi-simultaneously process; the scanner continuously described a pattern similar to a Lissajous figure projected into a regularly spaced grid of 7 by 7 nodes. The line-of-sight wind speed was measured simultaneously at the five stations for each scanner position. In effect, the speed of aerosols along the laser beam is estimated by evaluation of the Doppler frequency shift of back-scattered light at the interrogated positions. The laser operated with a pulse length of 200×10^{-9} s and the processing was performed with a range gate width of 100×10^{-9} s (see Appendix A). With this setup the probe length is approximately 34 m. The scanner movement and the lidar were setup to perform a fly-by measurement at each of the grid points. Scanning of flat planes parallel to the wind turbine rotor is achieved by updating the lidar ranges at each grid point continuously. To cover the measurement grid the angles in elevation and azimuth of the scanner were always below 20°; this means that for wind turbine yaw misalignment in normal operation, ranging from -10 to $+10°$, we expect a maximum of approximately 30° misalignment between the wind vector and the line of sight. Figure 5 shows an example of a measurement performed over ≈ 9 s. The intensity map represents the line-of-sight wind speed interpolated by means of a Delaunay triangulation on a grid with higher spatial resolution than the measurement grid.

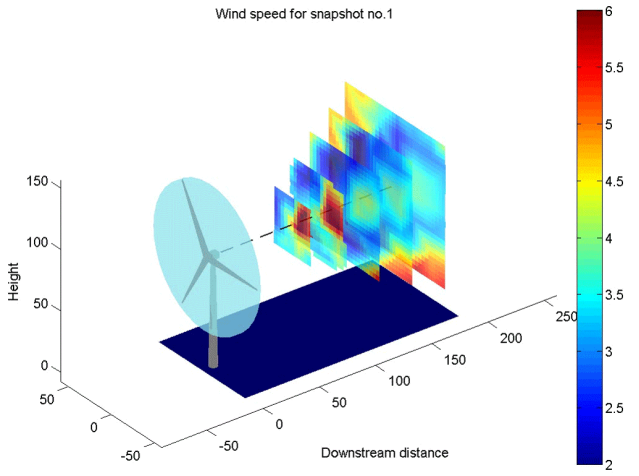

Figure 5. Example of snapshot taken with a nacelle-based lidar scanner. Measurement taken over ≈ 9 s. The colour map represents the line-of-sight wind speed in $[\mathrm{m\,s^{-1}}]$ interpolated into a high-resolution grid.

We performed wake tracking by fitting the template function (Eqs. 1 and 2) on such measured fields. This was done by applying a trust region algorithm[1] which has the ability to perform bounded optimisation, and in this way the domain of valid wake centre positions has been restricted to not exceed one rotor radius ($|\mu_y| \leq \mathcal{R}$ and $|\mu_z| \leq \mathcal{R}$).

3.2 Inflow conditions from meteorological mast at FINO1 platform

The wind farm inflow wind conditions for westerly winds were provided by the offshore meteorological mast FINO1. This is located to the north-west of the AV07 and is separated by a distance of approximately $8\,\mathcal{D}$ (Fig. 4). Wind speed vertical profiles are measured with calibrated cup anemometers at heights above the lowest astronomical tide (LAT) of 34.0, 41.5, 51.5, 61.5, 71.5, 81.5, 91.5, and 103.0 m. Additionally, three-dimensional sonic anemometers also provide wind speeds at three heights, namely, 41.5, 61.5, and 81.5 m. These two types of anemometers are located at different sides of the meteorological mast presenting different behaviour with respect to wake effects from the mast. To obtain suitable

[1] Specifically, we have used a trust region reflective algorithm implemented in the Optimisation Toolbox (version 6.4) of Matlab©: version 8.2.0.701, the MathWorks Inc., Natick, Massachusetts, 2013.

vertical profiles we processed the corrected cup and non-corrected sonic anemometers independently for each particular wind direction. The uncertainty in these signals is estimated to vary approximately between 2 and 4 % based on the information given by Westerhellweg et al. (2010, 2012). Moreover, we obtained the wind direction near hub height from the wind vane installed at 91.5 m LAT, where the uncertainty is estimated to vary between 2 and 6° (Westerhellweg et al., 2012). We selected data sets for wind directions where the turbine operates undisturbed by any of the neighbouring wind turbines, namely for wind directions in the sector between 209 and 330°. These angles are given in meteorological convention with 0° pointing to north and positive angles in a clockwise direction. For these conditions the average turbulence intensity, calculated on the basis of 10 min data as $I_o = \sigma_u/\overline{u}$, was $I_o = 0.165$ with a standard deviation of 0.049.

Finally, we performed an extrapolation of the vertical profile to estimate wind speeds above hub height and until the highest height measured by the lidar. This was performed using the measurements from 34.0 to 91.5 m LAT. For this, we assume that the profile follows the Businger–Dyer model for the diabatic boundary layer profile $u(z|u_*, z_o, L)$ as presented by Stull (1988). The model parameters, friction velocity u_*, roughness length z_o, and Monin–Obukhov length L, were estimated for each 10 min time series by performing a least-squares fit to the 10 min averages measured at FINO1.

A classification of the data with respect to atmospheric stability has been omitted since the obtained parameters presented high uncertainty. In effect, the results for L showed large variations and, in some cases, contradictory stability classification of consecutive data sets. Two factors can be the main origin of this: first, we used a short averaging period of 10 min, and second, there was a limitation in the measurement setup since the lowest measurement height was too high (above 30 m). These factors have been exposed by Cañadillas et al. (2011), who analysed stability effects at FINO1 in detail. Their analysis was performed with sonic anemometer data and the more elaborated covariance method. Nevertheless, they found a high scatter of the results when comparing against a bulk Richardson approach including mean meteorological measurements of 30 min and sea surface temperature data.

4 Results

4.1 Wake position statistics from selected single Gaussian tracking

During this experiment, we selected measurements for six consecutive days from 29 June 2011 at 00:00 UTC until 5 July 2011 at 00:00 UTC. During this period of westerly winds the wind turbine operated in free flow and mostly under wind speeds below rated speed, as can be seen in Fig. 6. This means that the data are representative of partial load

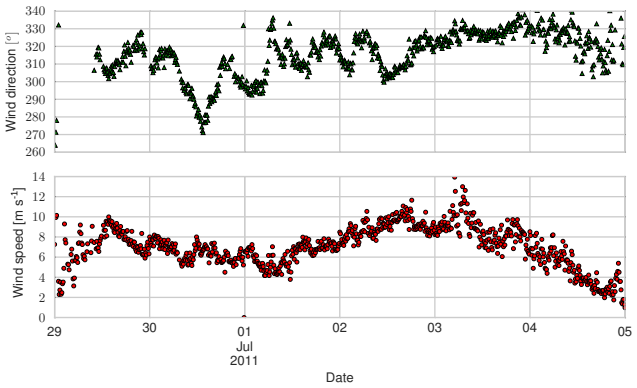

Figure 6. Inflow conditions: measured wind speed and wind direction at FINO1 at a height of 91.5 m LAT during a selected period from 29 June 2011 at 00:00 UTC until 5 July 2011 at 00:00 UTC.

conditions, where the thrust coefficient curve is relatively constant with values estimated to be above $c_T = 0.77$ during 75 % of the analysed time. Additionally, in regard to the yaw control of the turbine, during this time the turbine performs a maximum of two yaw corrections of some degrees in a 10 min period.

We selected the lidar data for the same dates and wind direction, furthermore we analysed them in 10 min blocks containing approximately 65 wind field snapshots. These data sets were checked concerning the back-scattered signal quality by filtering out low-quality data not complying with the lowest acceptable value of carrier-to-noise ratio, CNR $= -17$ dB.

Next, we tracked the wake position in each of the measured fields. First the wind speed was reconstructed by assuming full alignment of the wind vector with the rotor axis. Afterwards, the wake wind speed deficits were calculated by subtracting the inflow wind speed profile. This was obtained by averaging measurements at the FINO1 meteorological mast over 10 min and performing extrapolation as explained in Sect. 3.2.

Some tests have been performed with the extended template function in Eq. (2); this function has mainly been applied to a selected 10 min time series using the simplification that $\sigma_{y_2} = \sigma_{z_2}$. A qualitative comparison of the measured line-of-sight wind fields against the wind fields calculated with the fitted template functions showed better agreement of the double Gaussian than the single Gaussian template function. However, the obtained wake offsets were similar for both functions. Although the wake tracking with the double Gaussian template function was expected to be more robust in the nearer stations 1 and 2, we did not find a noticeable improvement in the convergence of the fitting algorithm for those stations. Due to this fact and an expected higher computational cost of the extended function, we applied the simpler function.

Table 1. Statistics of wake offset obtained with simple Gaussian tracking for a selected week. All values in lidar frame of reference are given in [m] except for the count.

	δ_{y_1}	δ_{y_2}	δ_{y_3}	δ_{y_4}	δ_{y_5}
Count	348	348	348	348	348
Mean	−1.8	−0.4	0.2	1.2	2.7
SD	4.6	1.8	1.9	3.4	5.3
Min	−12.1	−4.5	−4.8	−8.2	−10.0
Median	−1.7	−0.4	−0.2	1.3	3.0
Max	26.5	8.4	8.4	11.2	15.8

After performing wake tracking with this template, we selected 10 min time series of (μ_y, μ_z) where at least 70 % of the snapshots have been tracked successfully at each downstream station. This means that for that percentage of scans the fitting process has converged with the given bounds for all parameters and the convergence criteria. We have defined this ad hoc limit value to deal with unsuccessful fits. Primarily, we have identified three main sources of failed fitting attempts, namely a highly complex wind field, numerical issues of convergence, and nonexistence of wake deficit. The last one is related to the operational status of the turbine which at the time of applying the tracking procedure was not available. The results of sampled tests suggested a rather low effect of the first two sources; therefore, we assume that any large lost of tracked centres should be revealing a downtime of the turbine. In conclusion, the 70 % is expected to guarantee that in a 10 min period the turbine was under normal operation during that percentage of time. Afterwards, we calculated the 10 min averages $(\overline{\mu}_y, \overline{\mu}_z)$ at each station. Finally, for reconstruction of average wake paths, we selected only 10 min blocks for which data are available at all five stations and which complied with the inflow and signal quality criteria mentioned before. For this experiment, we found 348 ten-minute data sets complying with all these criteria. This is equivalent to ∼ 51 % rate of success, taking into account that 678 ten-minute data sets comply with the wind direction sector requirement.

The statistics of wake offset (δy_1) for the selected data are shown in Table 1. A linear regression through the mean values has given the function $\delta y_1 = 5x - 5$, where δy_1 is given in metres and x in $\mathcal{D}$. The slope is positive and equivalent to 2.6°. The data distribution can be seen in Fig. 7, where violin plots show the frequency distribution of wake offsets at each downstream station plotted together with the first, second, and third quartiles.

Additionally, we have made an estimation of the wake skewness, for the operational conditions of this experiment, whose typical values should lie below 3° as shown in Appendix B.

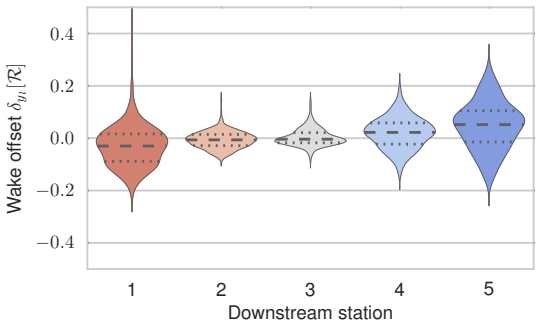

Figure 7. Violin plot of statistics showing the distribution of the frequency of the horizontal wake offset. The dashed lines represent the 25th, 50th, and 75th percentile. δy_1 is given in rotor radius [$\mathcal{R}$].

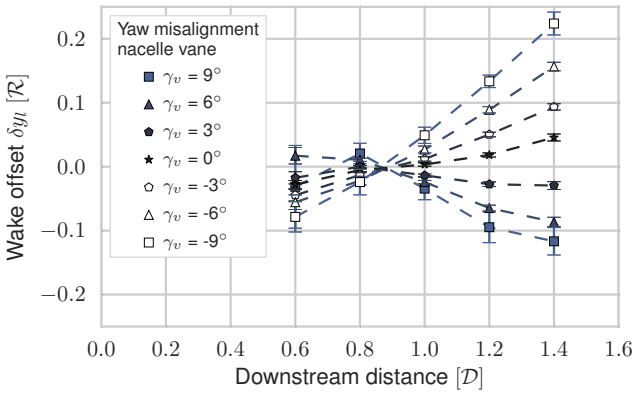

Figure 8. Mean near-wake paths measured by lidar wake tracking classified in 3° bins with respect to yaw misalignment measured with the nacelle vane. Bars show standard error on the mean.

4.2 Near-wake path dependency on yaw misalignment

The dependency of the mean near-wake path on yaw misalignment is shown in Fig. 8. This shows the results of classifying paths with respect to yaw misalignment based on the nacelle wind vane measurements. We have set an ad hoc bin size of 3° and performed averaging of all selected data at each downstream distance. The error bars present the standard error on the mean calculated as $s(\overline{\delta y_1}) = s_{\delta y_1}/\sqrt{N}$, where $s_{\delta y_1}$ is the standard deviation and N is the number of data points.

The mean yaw misalignment angles estimated from the mean near-wake paths (γ_w) are shown in Table 2. These were calculated by linear regression of the last three downstream stations (1.0, 1.2 and 1.4 $\mathcal{D}$), whereby γ_w is a transformation of the slope into degrees in the frame of reference of the rotor, namely $\gamma_w = -\gamma_{wt}$ (see Fig. 1). The difference between the vane and wake-tracking-based misalignment is calculated as $\Delta\gamma = \gamma_v - \gamma_w$ and its average over all bins is $\overline{\Delta\gamma} = +2.7°$.

Table 2. Results of estimation of yaw misalignment from wake tracking (γ_w) by linear regression through the last three stations of the near-wake path (1.0, 1.2, and 1.4 $\mathcal{D}$). Data classified in 3° bins with respect to yaw misalignment from nacelle vane (γ_v).

γ_v [°]	γ_w [°]	$\Delta\gamma$ [°]	Slope [m $\mathcal{D}^{-1}$]	Offset [m]	r^2 [–]
+9	+5.9	3.1	−11.9	9.6	0.9
+6	+4.5	1.5	−9.0	7.5	1.0
+3	+1.1	1.9	−2.3	1.4	0.8
0	−3.0	3.0	6.1	−6.0	1.0
−3	−5.8	2.8	11.8	−11.1	1.0
−6	−9.2	3.2	18.8	−17.3	1.0
−9	−12.3	3.3	25.4	−22.6	1.0

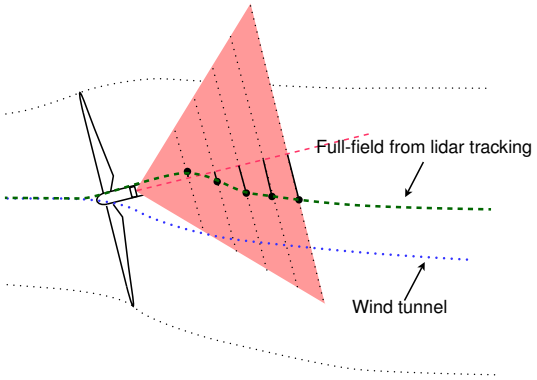

Figure 9. Diagram of our interpretation of the measured near-wake path for an individual yaw misalignment, showing what we call a deviation shift with respect to wind tunnel paths found in publications.

5 Discussion

5.1 Characteristics of full-field near-wake paths

Two main features can be observed in the near-wake paths obtained during this experiment (Fig. 8), namely what we call a shift of wake deviation and an asymmetry of the wake paths with reference to the nacelle longitudinal axis. We give the following interpretation to these results.

5.1.1 Shift of wake deviation

A feature of the obtained near-wake paths is their consistent convergence towards the centre at a downstream distance approximately at $x_1 \simeq 0.9\,\mathcal{D}$. We interpret this as if, just after this distance, the wake would deviate from the longitudinal axis of the nacelle as expected from the pure rotor thrust balance; therefore, we call this a wake deviation shift. A representation of this is presented in Fig. 9 for one hypothetical path. This contrasts with the wind tunnel observations (e.g. Grant et al., 1997; Haans et al., 2005; Medici and Dahlberg, 2003) which show that the near-wake paths meet at the nacelle area or very close to the rotor for horizontal yaw.

This is showing apparent differences in the pattern between the wake flow experienced in the published lab experiments and in our experiment. A hypothesis about this is that the blockage effect of the nacelle could be affecting the deficit in the centre but not at its radial limits. This could in fact lead to different results from both tracking procedures. In conclusion, this evidences a need for studies where the wake path estimation of both tracking techniques can be compared directly.

5.1.2 Near-wake path asymmetry

In the resulting paths we appreciate two regions, divided approximately at 0.9 $\mathcal{D}$, which show different characteristics of symmetry about the nacelle longitudinal axis. In the region between 0.6 and 0.8 $\mathcal{D}$ the paths show a tendency to lie towards the right side, when looking downstream. In contrast, at larger distances from 1.0 to 1.4 $\mathcal{D}$ the paths are distributed more evenly to both sides. In this region, however, there is some apparent and slight bias towards the left side. Although we can quantify an average between the yaw misalignment estimated with the wind vane and with the mean wake path ($\overline{\Delta\gamma} = +2.7°$), it is not possible for us to differentiate this as a pure, or a combination of, wind vane or lidar wake-tracking bias. In the following we contemplate some factors that affect this:

- Horizontally asymmetric mean inflow conditions: a steady horizontal wind shear could be responsible for a constantly deviated wake towards one side. However, we think that the probability of such inflow conditions is very low. Mainly, during the evaluated period of time, the wind direction range selected is relatively wide so that any local effects, due, for instance, to wind farm geometry, should not be persistent for the whole data set.

- Bias of the nacelle wind vane: we have checked the correlation between two sources of yaw misalignment, namely the nacelle wind vane and the difference between the wind direction measured at the meteorological mast FINO1 and the yaw position of the rotor. After performing a linear regression we obtained a bias of approximately +3° for the wind vane, which seems to coincide with the $\overline{\Delta\gamma} = +2.7°$.

- Biased wake-tracking method: the tracking method is applied here independently to each measured snapshot. In this process, the first guessed position in the minimisation algorithm is $\mu_y = 0$ and $\mu_z = 0$. Therefore, any bias of the method towards one direction could be given by the optimisation algorithm used. However, it does not seem plausible for it to have a predilection for one specific side. First, the function is symmetrical and

Table 3. Results of estimation of yaw misalignment (γ_w) by linear regression through last three points of the near-wake path (1.0, 1.2, and 1.4 $\mathcal{D}$). The data have been classified in 5° bins with respect to nacelle vane (γ_v).

γ_v [°]	γ_w [°]	$\Delta\gamma$ [°]	Slope [m $\mathcal{D}^{-1}$]	Offset m	r^2 –
10	5.9	4.1	−11.9	9.6	0.9
5	3.2	1.8	−6.6	5.3	1.0
0	−3.0	3.0	6.0	−6.0	1.0
−5	−7.8	2.8	15.8	−14.7	1.0
−10	−12.3	2.3	25.4	−22.6	1.0

smooth, and second, the optimising algorithm is not expected to have a preferred search direction. Therefore, any bias caused by the lidar wake tracking should be mainly caused by an error in orientation of the system on the nacelle. We have estimated an orientation error in the order of ±1° based on our knowledge of the lidar system and the mounting at the nacelle. However, the actual misalignment between the longitudinal axis of the lidar and the nacelle is unknown to us and a deviation from the estimated error could be possible. An accurate verification of this value could be performed through evaluation of nearby hard targets; however, this was practically not possible for us due to the lack of such external objects in the achievable range of our lidar system.

– Interaction of surrounding flow and rotating wake: a plausible hypothesis is that the near-wake path could show an asymmetry as a result of the interaction of wake flow rotation, vertical wind shear, and wake deficit. Such an effect has been observed experimentally in measurements analysed in the far wake in Trujillo et al. (2011). Furthermore, Dörenkämper (2015, p. 117) performed a numerical analysis of the effects of atmospheric stability through large eddy simulations, showing that the wake mean deviation is sensitive to the atmospheric stability conditions. Although the mentioned studies do not get into the near-wake region, we expect those far-wake effects to be also visible in the near region and therefore could be observable in our measurements.

Finally, despite the possible existence of such asymmetry, we expect that the implemented tracking method will still work effectively without generating a bias in the horizontal wake offset. This is due to the low misalignment angles analysed, for which no deformation of the mean wake deficit should be expected. We have not checked this directly but base our assumption on results of wind tunnel experiments. For instance, in the work of Krogstad and Adaramola (2012) we recognise that the shape of the wake changes for large yaw misalignments, yet we do not perceive any deformation between perfect alignment and $\gamma = 10°$.

5.2 Comparison against wind tunnel measurements

The shape of the near-wake paths measured during this campaign presents features which contrast with measurements of models in the literature. A qualitative comparison with a published wind tunnel experiment (Grant et al., 1997) has been performed in Fig. 10. The wake paths from wake tracking have been sorted in bins of $\gamma_v = 5°$ to make them comparable to the published paths. Additionally, the results are also summarised in Table 3.

In the wind tunnel experiment, the near-wake paths of a turbine model of 0.9 m diameter have been estimated by means of tip vortex tracking. The tip vortices have been observed and localised by means of the laser-sheet visualisation technique in an area ranging between ∼ 0.2 and ∼ 0.5 $\mathcal{D}$. Therefore these results are complementary to the measurements in this paper. In regard to the operational conditions of the model turbine, the thrust coefficient is not documented. However, it is inferred from the reported skewness that the thrust coefficient is relatively large. The wake offsets for the three-bladed model have been digitised and further processed for the comparison. First, the wake offsets have been normalised with the rotor radius, and second, they have been mirrored about the x axis due to the application of an opposite convention of yaw misalignment in both papers.

The most evident difference between both measurements is what we call a wake deviation shift. This phenomenon is not present in the wind tunnel measurements. Additionally, an asymmetry of the wake paths of the model turbine can be identified; however, such behaviour can not be easily stated in the full-field paths if the exact bias between yaw misalignment measurement and lidar orientation is not defined, as discussed in the last section. Finally, with the same background it is also not possible to draw conclusions on differences in wake skewness.

5.3 Wake-tracking performance

The wake-tracking method shows a robust behaviour for some measurements. First, the wake position can be estimated successfully even for measurements partially covering the wake cross section. Second, the wake can also be tracked for complex shapes which do not resemble exactly the predefined Gaussian shape. This is of advantage due to the highly complex character of the wake wind field. In spite of this, some limitations are seen in terms of overall availability, which amounts to 51.8 %. The main reason for this can be evidenced in the results shown in Fig. 7, where in the first two downstream stations (0.6 and 0.8 $\mathcal{D}$) the frequency distribution of wake offset shows larger changes than in the other stations further downstream. This can be attributed to failed convergence of the tracking process, rather than to a

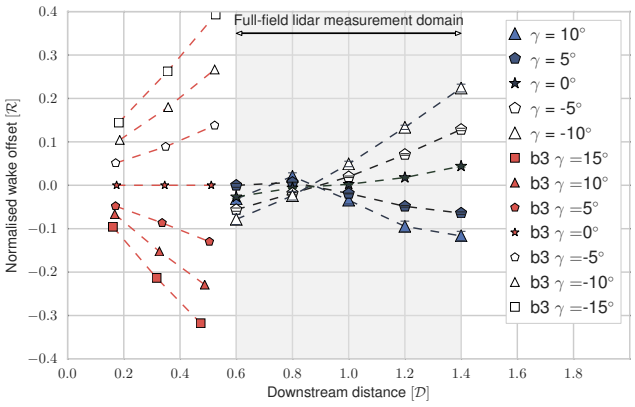

Figure 10. Comparison of published wind tunnel and full-field mean near-wake paths in the frame of reference of the turbine. The wind tunnel paths (from $\sim 0.2\,\mathcal{D}$ to $\sim 0.5\,\mathcal{D}$) have been digitised from Grant et al. (1997). Full-field paths from lidar averaged in 5° bins of yaw misalignment.

physical larger wake deviation at that position. This can be related to numerical issues, as well as to a extremely reduced measured area and a very complex flow field. As can be observed in Fig. 5, the unaffected flow at the nacelle level is very evident in the first stations and vanishes towards the end of the measurement domain at $1.4\,\mathcal{D}$. In this case, the nearer downstream stations 1 and 2 are affected to a greater degree than stations 3, 4, and 5, which show almost no effect from this complex flow. This suggests that to solve this problem the scanning of the very near wake must cover a larger area.

6 Conclusions

In this research we aimed at measuring in full scale the horizontal path followed by the wake of a wind turbine, and observe the effects of yaw misalignment on their trajectory in a region near the rotor which has not been documented in the literature. We successfully applied a lidar wake-tracking technique that has been tested previously to obtain far-wake paths. We have analysed the near wake of a 5 MW offshore wind turbine for distances between 0.6 and $1.4\,\mathcal{D}$ and under yaw misalignment arising in normal operation under free inflow conditions.

We identify a general limitation in the application of nacelle-based lidar for the analysis of the very near wake. Mainly, the performance of wake tracking is strongly diminished at the nearest distances to the rotor due to the reduced area which is interrogated by a lidar scanner. Despite the restrictions, we were able to obtain plausible full paths with a success rate slightly above 50 %. Furthermore, we succeeded in classifying distinctive wake paths with respect to yaw misalignment in angular bins of 3° in the range of $\pm 10.5°$. These results suggest that, excluding the bias, a consistent correspondence can be found between the tracked wake positions and yaw misalignment observed by the nacelle wind vane.

We appreciate an apparent asymmetry in the wake paths in reference to the nacelle longitudinal axis. Nonetheless, it is not possible for us to conclude whether this is due to orientation errors of the instruments or to actual systematic asymmetry of the wake paths. A more accurate estimation of lidar positioning and yaw misalignment than in our campaign is needed to disambiguate this issue.

In regard to the comparability against published results obtained in wind tunnel studies, we show that the wake paths are qualitatively different. A clear difference is that in our measurements all wake paths, in the lidar frame of reference, show a consistent convergence towards a downstream distance of approximately $0.9\,\mathcal{D}$. We interpret this as a wake deviation shift that has not been reported in wind tunnel studies.

Finally, the differences that we identify between the lab and our measurements lead us to conclude that there is need for research comparing wake paths obtained through tip vortex and wake-tracking techniques. We think that such work can give insight into the observed behaviour of our wake paths and would explain the discrepancies that we have found in this research.

Appendix A: Characteristics of lidar scanner system

Table A1 show the specifications of the lidar scanner system used for the measurements in this research.

Table A1. Characteristics of lidar scanner of the University of Stuttgart. Windcube WLS-7 version 1, extended with a scanning unit.

Property	Value
Wavelength	1.54×10^{-6} m
Repetition rate	10 000 Hz
Pulse energy	10×10^{-6} J
Pulse length (FWHM)	200×10^{-9} s $\rightarrow$ 30 m
Measurement range	40 to 200 m
Number of range gates	5
Data acquisition	
Photodiode sampling rate	250×10^{6} Hz
Range gate width	$\sim 0.1 \times 10^{-6}$ s $\rightarrow$ 15 m
Scanning	
Scanner	2 degrees of freedom
Target points trajectory	49
Period full trajectory	$\sim$ 9.125 s

Appendix B: Wake skewness

From theoretical considerations the wake deviation (χ_o) can be approximated as $\chi_o \simeq (0.6a + 1) \cdot \gamma$ (see vortex model in Burton et al., 2001), which derives into a skewness equal to $\psi \simeq 0.6a\,\gamma$. This behaviour is depicted in Fig. B1, where an approximate value of thrust coefficient C_T is given for the case of no misalignment. This is done taking into account that, based on the vortex model, the thrust coefficient is rather unaffected by yaw errors in the order of magnitude shown in Fig. B1.

The shaded area depicts approximately the yaw misalignment values which are covered during this experiment. As a consequence, the highest values of skewness that could be expected are below $\psi \simeq 3°$. However, this value already lies in the order of the typical uncertainty assumed for nacelle wind vanes. Therefore, we conclude that the wake skewness can not be resolved from pure yaw misalignment measurement by the standard wind vane at the nacelle in this experiment.

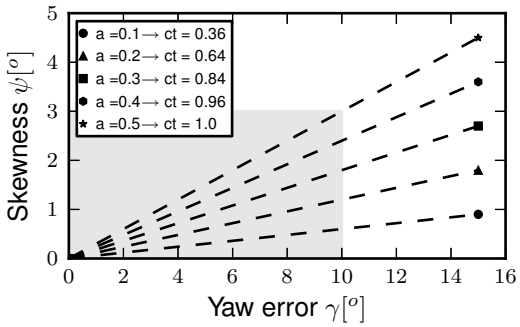

Figure B1. Representation of the effect of wind turbine misalignment (γ) on wake skewness (ψ).

Acknowledgements. We thank Adwen for the support during the setup of the measurement campaign. We are also grateful to Wilm Friedrichs and Frederik Berger at the University of Oldenburg for their proofreading and their valuable suggestions for improvement of this paper.

This research makes part of the German joint project "OWEA Loads – Probabilistic load description, monitoring and load reduction of future offshore wind turbines". It is supported by the Federal Ministry for Economic Affairs and Energy of Germany (BMWi) under contract no. 0325577B.

Edited by: J. Mann

References

Aitken, M. L., Banta, R. M., Pichugina, Y. L., and Lundquist, J. K.: Quantifying Wind Turbine Wake Characteristics from Scanning Remote Sensor Data, J. Atmos. Ocean. Tech., 31, 765–787, doi:10.1175/JTECH-D-13-00104.1, 2014.

Burton, T., Sharpe, D., Jenkins, N., and Bossanyi, E.: Wind Energy Handbook, John Wiley & Sons, Chichester, UK, 103–106, doi:10.1002/0470846062, 2001.

Cañadillas, B., Muñoz-Esparza, D., and Neumann, T.: Fluxes Estimation and the derivation of the atmospheric Stability at the offshore mast FINO1, in: EWEA Offshore, available at: http://www.dewi.de/dewi/fileadmin/pdf/publications/Publikations/PO312_CanadillasEOW2011paper.pdf (last access: 8 April 2016), 2011.

Dörenkämper, M.: An investigation of the atmospheric influence on spatial and temporal power fluctuations in offshore wind farms, PhD thesis, University of Oldenburg, Dr. Hut-Verlag, Munich, Germany, 168 pp., 2015.

España, G., Aubrun, S., Loyer, S., and Devinant, P.: Spatial study of the wake meandering using modelled wind turbines in a wind tunnel, Wind Energy, 14, 923–937, doi:10.1002/we.515, , 2011.

Fleming, P. A., Gebraad, P. M., Lee, S., van Wingerden, J.-W., Johnson, K., Churchfield, M., Michalakes, J., Spalart, P., and Moriarty, P.: Evaluating techniques for redirecting turbine wakes using SOWFA, Renewable Energy, 70, 211–218, doi:10.1016/j.renene.2014.02.015, 2014.

Fleming, P. A., Ning, A., Gebraad, P. M. O., and Dykes, K.: Wind plant system engineering through optimization of layout and yaw control, Wind Energy, 19, 329–344, doi:10.1002/we.1836, 2016.

Gebraad, P. M. O., Teeuwisse, F. W., van Wingerden, J. W., Fleming, P. A., Ruben, S. D., Marden, J. R., and Pao, L. Y.: Wind plant power optimization through yaw control using a parametric model for wake effects – a CFD simulation study, Wind Energy, 19, 95–114, doi:10.1002/we.1822, 2016.

Grant, I., Parkin, P., and Wang, X.: Optical vortex tracking studies of a horizontal axis wind turbine in yaw using laser-sheet, flow visualisation, Ex. Fluids, 23, 513–519, doi:10.1007/s003480050142, 1997.

Haans, W., Sant, T., van Kuik, G., and van Bussel, G.: Measurement of Tip Vortex Paths in the Wake of a HAWT Under Yawed Flow Conditions, J. Solar Energy Eng., 127, 456–463, doi:10.1115/1.2037092, 2005.

Jiménez, Á., Crespo, A., and Migoya, E.: Application of a LES technique to characterize the wake deflection of a wind turbine in yaw, Wind Energy, 13, 559–572, doi:10.1002/we.380, 2010.

Krogstad, P.-Å. and Adaramola, M. S.: Performance and near wake measurements of a model horizontal axis wind turbine, Wind Energy, 15, 743–756, doi:10.1002/we.502, 2012.

Machefaux, E., Larsen, G. C., Troldborg, N., Hansen, K. S., Angelou, N., Mikkelsen, T., and Mann, J.: Investigation of wake interaction using full-scale lidar measurements and large eddy simulation, Wind Energy, doi:10.1002/we.1936, in press, 2015.

Medici, D. and Dahlberg, J. Å.: Potential improvement of wind turbine array efficiency by active wake control (AWC), in: Proc. European Wind Energy Conference, 16–19 June 2003, Madrid, Spain, 2003.

Peña, A., Hasager, C. B., Lange, J., Anger, J., Badger, M., Bingöl, F., Bischoff, O., Cariou, J.-P., Dunne, F., Emeis, S., Harris, M., Hofsäss, M., Karagali, I., Laks, J., Larsen, S., Mann, J., Mikkelsen, T., Pao, L. Y., Pitter, M., Rettenmeier, A., Sathe, A., Scanzani, F., Schlipf, D., Simley, E., Slinger, C., Wagner, R., and Würth, I.: Remote Sensing for Wind Energy, E-Report 0029(EN), DTU Wind Energy, Roskilde, Denmark, 157–170, 2013.

Rockel, S., Camp, E., Schmidt, J., Peinke, J., Cal, R. B., and Hölling, M.: Experimental Study on Influence of Pitch Motion on the Wake of a Floating Wind Turbine Model, Energies, 7, 1954–1985, doi:10.3390/en7041954, 2014.

Stull, R. B.: An Introduction to Boundary Layer Meteorology, Kluwer Academic Publishers, Dordrecht, the Netherlands, 376–384, 1988.

Trabucchi, D., Trujillo, J. J., Steinfeld, G. Schneemann, J., and Kühn, M.: Simulation of measurements of wake dynamics with nacelle and ground based lidar wind scanners, in: Book of Abstracts Wake Conference, 8–9 June 2011, Visby, Sweden, 170–174, 2011.

Trujillo, J.-J., Bingoel, F., Larsen, G. C., Mann, J., and Kühn, M.: Light detection and ranging measurements of wake dynamics. Part II: two-dimensional scanning, Wind Energy, 14, 61–75, doi:10.1002/we.402, 2011.

Vermeer, L., Soerensen, J., and Crespo, A.: Wind turbine wake aerodynamics, Prog. Aerospace Sci., 39, 467–510, 2003.

Westerhellweg, A., Canadillas, B., Beeken, A., and Neumann, T.: One year of lidar measurements at FINO1-platform: comparison and verification to met-mast data, in: 10th German Wind Energy Conference – DEWEK 2010, 17–19 November 2010, Bremen, Germany, 2010.

Westerhellweg, A., Neumann, T., and Riedel, V.: FINO1 Mast Correction, DEWI Magazin, 40, 60–66, DEWI GmbH – Deutsches Windenergie Institut, Wilhelmshaven, Germany, 2012.